Dynamic Bandwidth Allocation for C-band Shared FBG Sensing and Telecommunications

Gabriel Cibira, Ivan Glesk

***Abstract*—The telecommunications data transfer in single-mode (SM) optical fiber (OF) of a passive optical network (PON) is managed by dynamic bandwidth allocation (DBA). In most internet of things (IoT) sensor network applications, both raw sensing signals and telecommunication data are transmitted in SM OFs, too. At the present time, this is not done in a shared SM OF. This paper presents a novel concept to share FBG sensing and telecommunication services (TS) in the optical C-band of the shared transmission. This concept is based on statistical detection and monitoring of fiber Bragg gratings (FBGs) sensing signals. The key steps of the proposed concept are FBG power spectral peaks statistical detection, monitoring of the FBGs dynamics and periodical estimation of TChs occupancy and availability. The proposed concept was demonstrated and validated using sensor network with a deployed group of FBG-based sensors, by implementing various static or dynamic approaches. By doing so, we achieved telecommunication channels (TChs) bandwidth availability approaching 80 %, compared to previously wasted bandwidth with availability at most 15.6 %. Experimental results showed that a DBA system with implemented dynamic TChs occupancy is a reliable way to share fiber bandwidth between both FBG sensing and TChs.**

***Index Terms*—dynamic bandwidth allocation, internet of things, optical fiber sensors, shared optical fiber, telecommunication services.**

I. Introduction to Dynamic Bandwidth Allocation

THE passive optical network (PON) timely supports and transfers various types of downstream and upstream data along its typical topology between central optical line terminal (OLT) and up to hundreds of users' optical network units (ONUs) or terminals (ONTs). To prevent interferences or backscatter in its single-mode (SM) optical fiber (OF), downstream and upstream traffic are often assigned to their separate wavebands. Typically, upstream requests for data, voice, video or other telecommunication services (TS) arrive in bursts from ONUs or ONTs to the OLT, which manages time-wavelength assignments applying dynamic bandwidth allocation (DBA) algorithms. The simplest way to manage the data upstream flow is to apply time-division multiple access (TDMA) protocol. Its low bandwidth utilization has been overcome by more efficient DBA algorithms, where time slots of some idle or low-utilization users are re-assigned to active users [1]. Here, ONUs buffer occupancy status is reported to statistical bandwidth multiplexing DBA algorithms, [2], [3], by grouping users by load. Some other DBA algorithms prefer transmission of packets without reporting, while prioritizing a class approach to guarantee ONUs bandwidth utilization, or weighting approach implementing fairness of priorities, quality of service (QoS), delay, loads etc. [4], [5].

Different modulation formats have been investigated, including their impact on QoS- or weighting-based DBA, [1], [2], [3], [4], [5], [6]. The statistical orthogonal frequency division multiple access (OFDMA) -based PONs with flexible bandwidth allocation increased their reach up to ×10 km, thanks to their dispersion tolerance and fine bandwidth granularity [7], [8]. Statistical algorithms are available for random upstream wavelengths assignment, to control multiband ONUs' lasers [2], [6], [8]. To eliminate spectral overlapping of ONUs' neighboring wavelengths, tunable lasers are used with reduced spectral widths [9]. Thermally stabilized lasers and wavelengths spectral separation of telecommunication channels (TChs) are also used [10]. Prioritization of QoS have been introduced for DBA, based on guaranteed criteria for TS classes, priority-queue scheduling, bandwidth requests, grade of service etc. [5], [9], [10].

Request-prediction algorithms aim to improve bandwidth utilization and PON throughput, to reduce delay and achieve fair transfer among users' data class [11], [12], [13]. Another DBA algorithms aim to minimize bandwidth waste using improved reporting of unused or inconsistent bandwidths, influencing wavelengths assignment, scheduling and polling processes [14]. Statistical 8-node × 8-wavelength multiplexing based on a simple arbitration has been designed in two-layer on-chip architecture [15]. Reinforcement learning predictive strategies are investigated to detect fast PON environmental changes [16]. Some dynamic wavelength and DBA algorithms aim to avoid or minimize frame re-arrangement problem when an ONU transmits in multiple TChs [17], or propose sleep mode algorithm based on PON load [18].

Recently, the revised IEEE 802.3-2018 Standard for Ethernet [19] was approved. In 2020, IEEE C/LM LAN/MAN standards committee approved the amendment IEEE Std 802.3ca: Physical layer specification and management parameters for 25 Gbps and 50 Gbps PONs [20] for Ethernet.

Manuscript received March xx, 2022; revised March xx, 2022 and April xx, 2022; accepted April xx, 2022. Date of publication April xx, 2022; date of current version May xx, 2022. This work was supported in part by the Slovak research and development agency (APVV) under grant 17-0631, in part by the European Union's Horizon 2020 Research and Innovation Program under the Marie Skłodowska-Curie under Grant 734331, and in part by Vedecka grantova agentura MSVVaS SR a SAV (VEGA) under grant 1/0113/22. *(Corresponding author: Gabriel Cibira.)*

Gabriel Cibira is with Institute of Aurel Stodola, Faculty of Electrical Engineering and Information Technology, University of Zilina, Univerzitna 1, 01026 Zilina, Slovakia (e-mail: gabriel.cibira@feit.uniza.sk).

Ivan Glesk is with the Electronic and Electrical Engineering Department, University of Strathclyde, Royal College Building, 204 George St, Glasgow, G1 1XW, United Kingdom (e-mail: ivan.glesk@strath.ac.uk).

Color versions of one or more figures in this article are available at https://doi.org/10.1109/JLT.2022.xxxxxxx.

Digital Object Identifier 10.1109/JLT.2022.xxxxxxx

Another ambitious project, the IEEE P802.3cs: Physical layers and management parameters for increased-reach point-to-multipoint Ethernet optical subscriber access (Super-PON), is currently being prepared, [20], [21], [22], [23], with separated C-band upstream and L-band downstream wavebands.

In IoT sensing applications, both raw FBG sensing signals and TS data are required to be transmitted. So far, they have been transmitted separately, e.g. in parallel SM OFs, as these services require reasonable signal-to-noise ratio (*SNR*) without interferences, and dissimilar time-wavelength management. The merging of FBG sensing and TS has not yet been considered. We propose a new efficient concept for DBA, based on statistical detection, FBGs tracking and secure periodical estimation of TChs occupancy and then availability, to share both FBG sensing and TS in the common G.652.D SM OF. It allows to reduce the conventionally pre-reserved operational bandwidth of sensing FBGs. A large portion of the previously wasted sensing bandwidth becomes available for the TS. We achieved the goal of high TChs availability with reliably low residual noise in TChs and low computational complexity.

The rest of the paper is organized as follows. Time-wavelength constraints and requirements for shared services are considered in section 2. Section 3 presents the proposed DBA procedures and specific approaches, including mathematical basis. Section 4 comprises simulation results, discussion and validation of the proposed DBA concept. Section 5 is a conclusion.

II. Time-Wavelength Constraints and Requirements for FBG Sensing and TS Shared in SM OF

Shared FBG sensing and TS in common SM OF depends on parameters of SM OF, scanning laser, FBG sensors and TS time-wavelength constrains and requirements. The scanning laser, a part of the sensing optical spectral analyzer (OSA), periodically transmits narrowband signals tuned along the scanned waveband. Each FBG reflects the scanning power in a bandwidth around FBG resonant wavelength λ_{FBG}. It is detected by OSA detector and indicated in the shape of FBG spectral peak. Any FBG represents a band-rejection filter where any TS can't be provided, because affected TChs suffer from significant power attenuation. However, the outside TS signals can pass with no reflection or attenuation. With respect of changing external influences, the λ_{FBG} shifts along its pre-designed operational wavelength window.

The basic parameters and notations used in this paper are listed in Table I and follow Recommendation ITU-T G.652 [24], IEEE standards [19], [20], [21], papers [22], [23], OSA/FBG sensors datasheets [25] and include our own measurements and calculations.

A. Upstream time-wavelength constraints

The PON upstream data traffic mostly arise randomly in many short-time bursts. Strictly adhering to prescribed standards [19], [20], [21], timed data frames are transmitted from ONUs or ONTs within time slots to OLT in TCh assigned by specific DBA algorithms (see section I).

Let the Super-PON is a reference type of TS network for this paper. Besides of basic parameters listed in Table I, it admits stabilized power ripple below 2 dB around TCh central wavelength $\Delta\lambda_{TCh} = \pm 15$ GHz of the total TCh bandwidth $B_{TCh} = 100$ GHz [22], [23]. Burst synchronization sequences of several prepared 257-bit data blocks (up to 56) and 10 parity blocks are sent in codewords organized into upstream data frames. The ONTs buffers may transmit data only in a given time slot and in the assigned TCh, managed by DBA algorithm. Up to 1024 users' ONTs devices per SM OF with reach of up to 50 km should operate in 32 upstream TChs [22].

Concluding for this subsection: The Super-PON upstream SM OF needs an appropriate DBA algorithm. When sharing FBG sensing and TS bandwidth, it is necessary to manage the upstream TS for the next sensing period. It is important to synchronize the narrowband scanning laser and DBA system and periodically update the TChs occupancy matrix.

B. Laser scanning requirements

During the laser scanning, the pulse power increases the background noise level. Therefore, it will be impossible to operate TS of impacted wavelengths in affected TChs. Suitable short-pulse narrowband tunable lasers for FBG sensing or TS applications were described by [26], [27], [28], [29], [30]. Fig. 1(a) shows an example of sweeping by a narrowband laser in the C-band during $T_{scan} \approx 2$ s. We can see that $n_{\lambda C} = 436$ of narrowband wavelengths periodically occupy the C-band. The fixed indicated wavelengths λ_i are represented by black vertical lines. The red vertical lines represent the central wavelengths of the Super-PON upstream TChs, while blue and dashed green verticals represent edges.

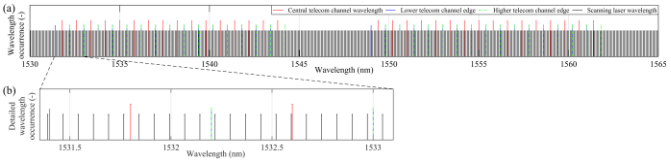

Fig. 1. Discrete spectrum of the narrowband tunable scanning laser in C-band: (a) scanning wavelengths accompanied by TChs, (b) detailed zoom in.

Using values from Table I we can find that a wavelength is occupied by the laser sweeping for a duration of $T_{sp\ laser} \approx 3.766$ ms. Each TCh is affected by $n_{\lambda\ TCh} \approx 10$ laser wavelengths, see Fig. 1(b). This therefore lasts for $T_{TCh} \approx n_{\lambda\ TCh} \times T_{sp\ laser} \approx 37.66$ ms. Consequently, 32 upstream TChs are affected by $n_{\lambda\ TChs} \sim n_{TCh} \times n_{\lambda\ TCh} = 32 \times 10 = 320$ wavelengths. Therefore, TChs occupancy lasts for $T_{TChs} \approx 32 \times T_{TCh} \approx 32 \times 0.0377 \approx 1.21$ s. Due to the sweeping, only one of 32 TChs will be occupied simultaneously during the sweeping interval. Thus the narrowband scanning laser leads to $\Xi_{TChs\ laser\ \%} = 1 / (n_{C1\ Tchs} + n_{C2\ Tchs}) = 1/32 = 3.125$ % TChs occupancy within TS allocated time, per period.

C. FBG sensing constraints

In general, FBG sensor systems rely on inter-period monitoring of shifts of the FBG resonance wavelength which occur due to external strain, pressure or temperature changes, [31], [32], [33]. Often, FBGs are inserted in series along the SM OF and firmly connected to the measured subject [34]. The reflected power $P_{dB\ i}$ (belonging to the B_{FBG}) significantly surpass the background noise N_{dB} and is detected by OSA analyzer, [31], [32]. It is measured and indicated by OSA at discrete number of wavelengths $n_{\lambda\ FBG}$ around λ_{FBG} [35]. Local

external temperature fluctuations are often compensated by coupled temperature compensation FBG in a common encapsulation [36], [37]. Different FBG sensors, sensing principles, FBG distribution techniques, technologies for high spatial resolution, sufficient accuracy and multi-peak demodulation algorithms are on hands for groups of FBGs applied in structural subjects health monitoring systems [34], [35], [38], [39], [40], [41].

Fig. 2 illustrates conventional sensing example of fixed non-overlapping operational wavelength windows (one per each FBG) obtained using G.652.D SM OF [24], OSA and FBG sensors [25] (also see Table I). Two coupled FBG sensors produce 4 power spectral peaks A, B, C, D located in their pre-designed operational wavelength windows depicted by dashed blue or red rectangles as shown in Fig. 2. We can see that the temperature sensing A-FBG operates in a narrower wavelength window than the strain sensing B-FBG. Similarly, for C and D FBGs used in the second coupled sensor. The orange vertical lines in Fig. 2 represent central wavelengths of the accompanied Super-PON TChs. Considering reasonable residual noise of the spectral peaks, each FBG occupies about 15 to 25 wavelengths. In summary, FBG windows overlap TChs so that only 5 of 32 i.e. 15.6 % of TChs are safely outside of FBG sensing. In real sensing applications, the OSA often monitors the only wavelength $\lambda_{Pmax\,i,j}$ at the FBG power maximum, thus the four maxima around + 17 dB level above the mean background noise N_{dB} have about $SNR_{dB} \approx +17$ dB in this example.

Fig. 3 illustrates single period of TChs occupancy merging laser wavelengths sweep with FBG occupancy. Black vertical lines represent TChs edges and the horizontal gray lines the timing of the laser and FBGs behavior, accordingly. Fig. 3(a) and 3(c) depict time-wavelength sweep of the narrowband tunable laser described in subsection II. *B.* resulting into diagonal "staircase" across of the TChs occupancy matrix shown in Fig. 3(d). Comparing Fig. 3(b) and Fig. 3(d), one can see that A-FBG does not interfere with any TCh, C-FBG with one, B and D FBGs at most with two.

Any external environmental parameters changes impose the FBGs' spectral peak shifts within their pre-determined operational wavelength windows. This effect is shown in multiple wavelength scan in Fig. 4. The temperature A-FBG stays in its original position. The C-FBG shifts very slowly from TChs to the guard zone thus not interfering any adjacent TCh. The B-FBG overlaps up to 6 TChs while D-FBG shifts a bit more and overlaps up to 9 TChs. The B and D FBGs shift slowly, meaning just up to 5 wavelengths per period which is half of the TCh bandwidth but it is less than half of the B_{FBG} at considered threshold level $\tau_{dB} \approx -68$ dB. The strained D-FBG fully relaxes in last period and undergoes blue shift (towards the C-FBG). Please note, some residual noise still remains in TChs below the $\tau_{dB} \approx -68$ dB.

In conclusion, each of sensing FBGs spectral peaks will occupy only $n_{\lambda\,FBG}$ wavelengths. Sensing with modest number n_{FBGs} of FBGs will occupy only a fraction $\Xi_{\lambda\,C\,FBGs}$ $(= n_{\lambda\,FBG} \times n_{FBGs})$ of the total number $n_{\lambda\,C}$ of wavelengths within the C-band. The unoccupied wavelength slots $\Psi_{\lambda\,C\,TS}$ $(\leq (n_{\lambda\,C} - \Xi_{\lambda\,C\,FBGs} - \Xi_{\lambda\,laser}))$ are not used in the currently implemented conventional sensing. However, this wasted bandwidth could be made available for shared TS or other services in the common SM OF.

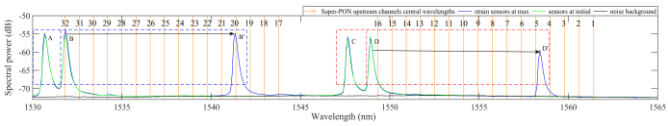

Fig. 2. FBG responses deployed during single period of sensing along C-band in SM OF from two coupled FBG sensors.

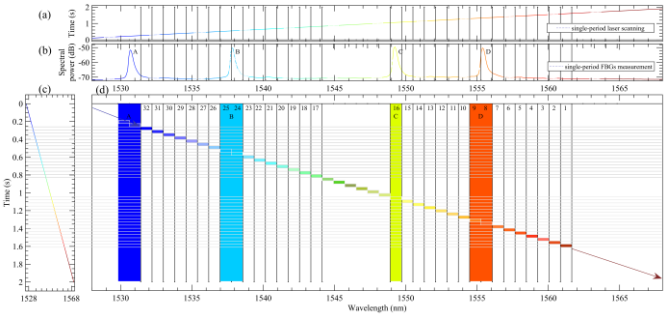

Fig. 3. FBG sensing occupancy during $T_{scan} = 2$ s single period, obtained from narrowband linearly tuned scanning laser and two coupled FBG sensors in C-band: (a) linearly tuned time-wavelength laser scanning, (b) FBGs spectral peaks deployment, (c) linearly tuned wavelength-time laser scanning, (d) merged sensing occupancy matrix.

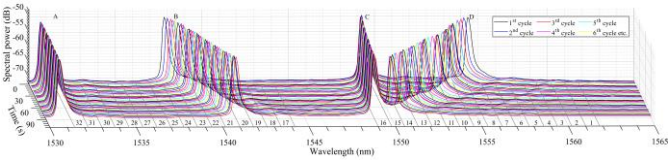

Fig. 4. Superimposed multi-period scan showing FBGs spectral peaks shifts. This was obtained as a combination of 45 scans lasting 45 × 2 s = 90 s.

III. Concept of FBG Sensing and TS Shared in SM OF

Based on section II., the behavior of the scanning laser and the FBGs spectral peaks would significantly influence on DBA management of TS. Therefore, both must be taken into account before the DBA algorithm can be used.

First, we derived the a-posteriori matrices of TChs occupancy $\Xi_{TChs\,j}$ then availability $\Psi_{TChs\,j}$ for the j^{th} period, just after the $(j\text{-}1)^{th}$ sensing period. To improve the reliability of the processing, the statistical detection is taken into account. To lower the risk of not capturing the exact inter-period dynamics of the FBGs spectral peaks, we developed several approaches for extended occupancy estimation. This depends on sensing application and background noise fluctuations. Then we designed the algorithm for DBA taking into account minimized computational demands by following steps:

1. background noise $N_{dB\,(j-1)}$ acquisition from $(j\text{-}1)^{th}$ period,
2. detection threshold $\tau_{dB\,(i-1)}$ calculation from $(j\text{-}1)^{th}$ period,
3. wavelengths occupancy $\Xi_{\lambda\,i,(j-1)}$ detection from $(j\text{-}1)^{th}$ period,
4. prohibited wavelengths $\Xi_{\lambda\,j}$ and TChs $\Xi_{TChs\,j}$ identification for current j^{th} period,
5. TChs availability $\Psi_{TChs\,j}$ computation for j^{th} period,
6. TChs availability validation for j^{th} period, $\Psi_{TChs\%\,j}$ or $\Xi_{TChs\%\,j}$, $N_{res\,dB\,j} < \tau_{dB\,(j-1)}$.

TABLE I
BASIC PARAMETERS NOTATIONS

Device / service		Parameter			
		Notation	Unit	Value	Description and parameters conversion
G.652.D SM OF[24]		B_C	*nm*	35	C-band operational bandwidth: $B_C = \lambda_{C\,max} - \lambda_{C\,min}$
		$\lambda_{C\,min}$	*nm*	1530	minimum wavelength of C-band
		$\lambda_{C\,max}$	*nm*	1565	maximum wavelength of C-band
		P_{att}	*dB/km*	≤ 0.275	power attenuation coefficient in C-band per km [24]
		$l_{OF\,max}$	*m*	< 50 000	maximum length of OF [22]
		l_{OF}	*m*	10 000	OF length used in experiments
Super-PON TS upstream [22]	C	B_{TCh}	*GHz*	~ 100	bandwidth of telecommunications channel
		$\Delta\lambda_{TCh}$	*nm*	~ 0.8	bandwidth of telecommunications channel
	C-band 2	B_{C2}	*nm*	12.76	bandwidth of 17 to 32 TChs: $B_{C2} = \lambda_{C2\,max} - \lambda_{C2\,min} = \Delta\lambda_{C2\,TChs} \times n_{C2\,TChs}$
		$\lambda_{C2\,min}$	*nm*	~ 1531.42	minimum wavelength
		$\lambda_{C2\,max}$	*nm*	~ 1544.18	maximum wavelength
		$\Delta\lambda_{C2\,TChs}$	*nm*	~ 0.7975	mean TChs bandwidth: $\Delta\lambda_{C2\,TCh} = (\lambda_{C2\,max} - \lambda_{C2\,min}) / n_{C2\,TChs}$
		$n_{C2\,Tchs}$	*pcs*	16	number of TChs
	C-band 1	B_{C1}	*nm*	12.84	bandwidth of 1 to 16 TChs: $B_{C1} = \lambda_{C1\,max} - \lambda_{C1\,min} = \Delta\lambda_{C1\,TChs} \times n_{C1\,TChs}$
		$\lambda_{C1\,min}$	*nm*	~ 1548.95	minimum wavelength
		$\lambda_{C1\,max}$	*nm*	~ 1561.79	maximum wavelength
		$\Delta\lambda_{C1\,TChs}$	*nm*	~ 0.8025	mean TChs bandwidth: $\Delta\lambda_{C1\,TCh} = (\lambda_{C1\,max} - \lambda_{C1\,min}) / n_{C1\,TChs}$
		$n_{C1\,TChs}$	*pcs*	16	number of TChs
OSA S-Line 400 [25]		T_{scan}	*s*	≈ 2	scanning period of the wavelength tuneable laser
		$\lambda_{min\,laser}$	*nm*	1525.6	minimum wavelength of linearly tuned laser (beyond C-band)
		$\lambda_{max\,laser}$	*nm*	1568.3	maximum wavelength of linearly tuned laser (beyond C-band)
		$\Delta\lambda_{laser}$	*nm*	≈ 0.08	resolution i.e. wavelength step: $\Delta\lambda_{laser} \approx (\lambda_{max\,laser} - \lambda_{min\,laser}) / (n_{\lambda\,scan} - 1)$
		$T_{sp\,laser}$	*ms*	≈ 3.766	laser period: $T_{sp\,laser} = T_{scan} / (n_{\lambda\,scan} - 1)$
		T_{TCh}	*ms*	≈ 37.7	duration of laser scanning in a telecommunication channel: $T_{TCh} \approx n_{\lambda\,TCh} \times T_{sp\,laser}$
		T_{TChs}	*ms*	≈ 1210	duration of laser scanning in 32 telecommunication channels: $T_{TChs} \approx (n_{C1TCh} + n_{C2TCh}) \times T_{TCh}$
		$n_{\lambda\,scan}$	*pcs*	532	number of scanning wavelengths per scanning period: $n_{\lambda\,scan} = (\lambda_{max\,laser} - \lambda_{min\,laser}) / \Delta\lambda_{laser}$
		$n_{\lambda\,C}$	*pcs*	436	number of wavelengths per C-band: $n_{\lambda\,C} = B_C / \Delta\lambda_{laser}$
		$n_{\lambda\,TCh}$	*pcs*	~ 10	number of wavelengths per TCh: $n_{\lambda\,TCh} = \Delta\lambda_{TCh} / \Delta\lambda_{laser}$
		λ_i	*nm*	1530 to 1565	measured i^{th} wavelength of $n_{\lambda\,C}$ scanning wavelengths along C-band: $\lambda_i = \lambda_{C\,min} + i \times \Delta\lambda_{laser}$
		$\lambda_{i,j}$ or $\lambda_{i,(j-1)}$	*nm*	1530 to 1565	measured i^{th} wavelength along j^{th} or $(j–1)^{th}$ scanning period
		$P_{d\,min}$	*dB*	< −70	detectable minimum power
SC-01/T cable strain coupled FBG sensors [25]	power, wavelength, time	n_{FBGs}	*pcs*	4	number of sensing FBGs in C-band SM OF
		$\lambda_{A\text{-}FBG}$	*nm*	1530.9	resonant wavelength of temperature compensating A-FBG at + 20°C
		$\lambda_{C\text{-}FBG}$	*nm*	1547.9	resonant wavelength of temperature compensating C-FBG at + 20°C
		$\lambda_{B\text{-}FBG}$	*nm*	1531.9	resonant wavelength of strain B-FBG at relaxed position
		$\lambda_{D\text{-}FBG}$	*nm*	1548.9	resonant wavelength of strain D-FBG at relaxed position
		$\lambda_{Pmax\,i,j}$	*nm*	1530 to 1565	measured resonant wavelength referred to FBG peak maximum, at i^{th} wavelength in j^{th} period
		B_{FBG}	*nm*	~ (0.6 to 2.1)	bandwidth of single FBG spectral peak: $B_{FBG} = (n_{\lambda\,FBG} - 1) \times \Delta\lambda_{laser}$
		$n_{\lambda\,FBG}$	*pcs*	~ (8 to 25)	number of reflected/measured wavelengths per FBG spectral peak, depending on detection threshold
		$\Delta\lambda_{i,j}$	*nm*	± (0 to 0.5)	FBG wavelength shift during T_{scan}, at i^{th} wavelength along j^{th} period compared to $(i±k)^{th}$ wavelength along previous $(j\text{-}1)^{th}$ period: $\Delta\lambda_{i,j} = \lambda_{Pmax\,i,j} - \lambda_{Pmax\,(i±k),(j-1)}$
		$P_{dB\,i}$ /$P_{dB\,\dots\,i,(j-1)}$/	*dB*	− 72 to − 45	power level at i^{th} wavelength /along (j-1)th period/: $P_{dB\,i} = 10\,log_{10}\,P_{W\,i}$; $P_{W\,i} = 10^{PdB\,i\,/\,10}$
		N_{dB}	*dB*	− 72 to − 70	mean background noise level: $N_{dB} = 10\,log_{10}\,N_W$; $N_W = 10^{NdB\,/\,10}$
		SNR_{dB}	*dB*	5 to 25	signal-to-noise ratio: $SNR_{dB} = 10\,log_{10}\,(P_{W\,i} / N_W) = P_{dB\,i} - N_{dB}$; $SNR = P_{W\,i} / N_W = 10^{SNRdB\,/\,10}$
	operation	Δt	°C	– 20 to + 60	temperature operational range
		t_{acc}	°C	< 1	temperature accuracy of temperature compensating FBGs
		t_{prec}	°C	± 0.3	temperature precision of temperature compensating FBGs
		$\Delta\varepsilon$	$\mu\varepsilon$	± 5000	strain range of strain FBGs
		ε_{acc}	%	< 0.18	strain accuracy of strain FBGs, of full scale range
Key calculated parameters		τ_{dB}	*dB*	– 68	constant threshold level (also reference limit for residual noise validation)
		$\tau_{dB\,(j-1)}$	*dB*	–	variable threshold level obtained from $N_{dB\,(j-1)}$ of $(j–1)^{th}$ period
		$N_{dB\,add}$	*dB*	–	additional component to the variable threshold
		$\Xi_{\lambda\,i,(j-1)}$	*LOG*	*LOG*0 / *LOG*1	occupancy matrix of i^{th} wavelength of $(j–1)^{th}$ period
		$\Xi_{TCh\,o,(j-1)}$	*LOG*	*LOG*0 / *LOG*1	occupancy matrix of o^{th} TCh of $(j–1)^{th}$ period
		$\Xi_{TChs\,j}$	*LOG*	*LOG*0 / *LOG*1	occupancy estimation of TChs for j^{th} period
		$\Psi_{TChs\,j}$	*LOG*	*LOG*0 / *LOG*1	availability estimation of TChs for j^{th} period
		$N_{dB\,res\,i,j}$	*dB*	< τ_{dB}	residual noise occurred in TChs at i^{th} position in j^{th} period after statistical detection

1. The mean background noise $N_{dB\,(j-1)}$ acquisition from the previous $(j-1)^{th}$ sensing period can be executed through several different ways:

   a. in some large-scale applications consisted of several SM OFs, the FBG sensing can be executed by shared OSA; here, TS should be temporarily suspended from the particular SM OF or re-routed to other SM OFs during the laser scanning; next, the detected FBGs power at their wavelengths must be excluded from the sum of background noise $P_{dB\,i,(j-1)}$ along C-band thus the mean $N_{dB\,(j-1)}$ is:

$$N_{dB(j-1)} = \frac{\sum_{i=1}^{n_{\lambda C}} P_{dB\,i,(j-1)} - \sum_{i=1}^{n_{\lambda FBGs}} P_{dB\,i,(j-1)}}{n_{\lambda\,C} - n_{\lambda\,FBGs}}, \quad (1)$$

   b. usually, the TS are provided continuously in upstream TChs; therefore, the power $P_{dB\,TChs\,i,(j-1)}$ along their wavelengths $n_{\lambda\,TCh}$ must be excluded from the $N_{dB\,(j-1)}$; besides exclusions in approach 1.a., we exclude temporarily all collateral services from guard zones to suspend its power $P_{dB\,guard\,i,(j-1)}$ from the $N_{dB\,(j-1)}$ that is:

$$N_{dB(j-1)} = \frac{\sum_{i=1}^{n_{\lambda C}} P_{dB\,i,(j-1)} - \sum_{i=1}^{n_{\lambda FBGs}} P_{dB\,i,(j-1)} - \sum_{i=1}^{n_{\lambda guard}} P_{dB\,i,(j-1)}}{n_{\lambda\,C} - n_{\lambda\,FBGs} - n_{\lambda\,guard}}, \quad (2)$$

   c. if FBGs bandwidths and TS are out of a specific bandwidth fraction in guard zones, the local noise acquisition (2) is modified to fractional case with the noise acquisition performed from a fraction $n_{\lambda\,fract}$ of wavelengths without services:

$$N_{dB(j-1)} = \frac{\sum_{i=1}^{n_{\lambda fract}} P_{dB\,i,(j-1)}}{n_{\lambda\,fract}}, \quad (3)$$

   d. to respect the SM OF attenuation characteristics along the C-band, we recommend to involve the noise trend function $f(N_{dB\,i,(j-1)})$ into (1), (2), (3); for example, (3) can be adopted by $f(N_{dB\,i,(j-1)})$ offset as follows:

$$N_{dB(j-1)} = \frac{\sum_{i=1}^{n_{\lambda fract}} P_{dB\,i,(j-1)} \pm f\left(N_{dB\,i,(j-1)}\right)}{n_{\lambda\,fract}}. \quad (4)$$

2. The background noise might fluctuate period-by-period. We recommend that the detection threshold $\tau_{dB\,(j-1)}$, a statistical function of the $(j-1)^{th}$ period, follows its inter-period fluctuations. The $\tau_{dB\,(j-1)}$ brings sufficient bandwidth utilization of the SM OF and plays a key role in ensuring the reliability of not interference of services for the next j^{th} period. The $\tau_{dB\,(j-1)}$ consists of $N_{dB\,(j-1)}$ (from step 1) and additional noise-based component which allows the $\tau_{dB\,(j-1)}$ to be liberal or stricter. The additional noise-based components can be included in one of the following ways:

   a. by adding permanent $N_{dB\,add} = const$ into the mean $N_{dB\,(j-1)}$ (so that the $\tau_{dB\,(j-1)}$ will inter-periodically depend only on the $N_{dB\,(j-1)}$ fluctuations); this is recommended approach for applications with stable background noise; such a simple adaptive threshold is:

$$\tau_{dB(j-1)} = N_{dB(j-1)} + N_{dB\,add} = N_{dB(j-1)} + const_{dB}, \quad (5)$$

   b. by adding variable $N_{dB\,add} = var$ based on intra-period fluctuations to the inter-period $N_{dB\,(j-1)}$; the variable component should be simply computable like statistical dispersion $D_{NdB\,(j-1)}$ that can be obtained just after the noise acquisition step 1; besides, this component might be parametrized by weight w; some increased $\tau_{dB\,(j-1)}$ is liberal to residual noise thus the noise increase in TChs and wavelengths occupancy will decrease; the liberal approach fits for TS where a small SNR is still acceptable in TChs; vice-versa, we recommend to use lowered stricter $\tau_{dB\,(j-1)}$ for less power stable cases; the intra- and inter-period -based adaptive threshold is:

$$\tau_{dB(j-1)} = N_{dB(j-1)} + N_{dB\,add\,(j-1)} = N_{dB(j-1)} + w \times D_{N_{dB}\,(j-1)}. \quad (6)$$

3. Wavelengths occupancy matrix $\Xi_{\lambda\,i,(j-1)}$ is obtained by threshold detection for the $(j-1)^{th}$ period, by comparing individual wavelengths power $P_{dB\,i,(j-1)}$ to the $\tau_{dB\,(j-1)}$. Preliminary, the $\Xi_{\lambda\,i,(j-1)} = LOG0$ (logical value) i.e. all wavelengths are considered unoccupied. If $P_{dB\,i,(j-1)}$ belongs to the FBG spectral peak s sequence of wavelengths from $\lambda_{i,(j-1)}$ to $\lambda_{(i+s),(j-1)}$, it exceeds the $\tau_{dB\,(j-1)}$, indicated occupied by $\Xi_{\lambda\,i,(j-1)} = LOG1$ at i^{th} to $(i+s)^{th}$ positions of the $(j-1)^{th}$ period as follows:

$$\forall\left\{P_{i,(j-1)} \ldots P_{(i+s),(j-1)}\right\}\left\{> \tau_{dB(j-1)} \;\therefore\; \therefore\; \left\{\Xi_{\lambda\,i,(j-1)} \ldots \Xi_{\lambda\,(i+s),(j-1)}\right\} \equiv LOG1. \right. \quad (7)$$

4. Depending on the FBGs dynamics, upstream requests and general reliability strategy, occupancy matrices for wavelengths $\Xi_{\lambda\,i,j}$ and TChs $\Xi_{TChs,j}$ summarize the $(j-1)^{th}$ occupancy and adjacent prohibited wavelengths or TChs. TS will be not allowed during the running j^{th} sensing period. Based on (7) in above step 3., we recommend the wavelength-based prohibition to be executed by one of the following ways:

   a. in minor FBGs shifts and static background noise situations, the estimated $\Xi_{\lambda\,i,j}$ (8) must include $LOG1$ occupancy values from $\Xi_{\lambda\,i,(j-1)}$ (7). In addition, TS should be forbidden for k neighboring wavelengths (9) due to possible bilateral FBG shifts during j^{th} period. Finally, the TChs occupancy $\Xi_{TChs\,1\ldots32,j}$ is determined (10):

$$\forall\left\{\Xi_{\lambda i,(j-1)}\right\} \equiv LOG1 \;\;\therefore\;\; \left\{\Xi_{\lambda i,j}\right\} \equiv LOG1, \quad (8)$$

$$\exists\left\{\left(\Xi_{\lambda i,(j-1)} \equiv LOG1\right) \in \left(B_{C1} \cup B_{C2}\right)\right\} \;\Rightarrow\; \Rightarrow \left\{\Xi_{\lambda(i-k),j} \ldots \Xi_{\lambda(i+k+s),j}\right\} \equiv LOG1, \quad (9)$$

$$\forall\left\{\Xi_{\lambda(i-k)\ldots(i+k+s),j} \in \left(\Delta\lambda_{TCh\,1\ldots16} \cup \Delta\lambda_{TCh\,17\ldots32}\right)\right\} \equiv LOG1 \;\therefore\; \therefore\; \left\{\Xi_{TChs\;o\in(1\ldots32),j}\right\} \equiv LOG1, \quad (10)$$

   b. in some cases, where significant "unexpected" FBGs shifts or interference will occur, the occupancy matrix $\Xi_{\lambda\,i,j}$ will prohibit a proportionally larger number of

wavelengths resulting in r-number of adjacent TChs around o^{th} TCh being prohibited during the j^{th} period; resulting from the previous approach 4.a., (8), a coarse-grained approach is applied:

$$\exists\left\{\left(\Xi_{\lambda\, i,(j-1)} \equiv LOG1\right) \in \left(\Delta\lambda_{TCh\ 1\ldots16} \cup \Delta\lambda_{TCh\ 17\ldots32}\right)\right\} \Rightarrow \Rightarrow \left\{\Xi_{TChs\ o\in(1\ldots32),\,j}\right\} \equiv LOG1, \tag{11}$$

$$\forall\left\{\Xi_{TChs\ o\in(1\ldots32),\,j}\right\} \equiv LOG1 \quad \therefore \quad \left\{\Xi_{TChs\ (o\pm r),\,j}\right\} \equiv LOG1, \tag{12}$$

c. when significant FBGs peak shifts are expected, then FBGs tracking is recommended as follows: bilateral approach 4.a. is applied from (8) and (9) for a small number of wavelengths around static FBGs peaks followed by unilateral tracking approach to ensure safe number of prohibited wavelengths or TChs in an FBG shifting direction; this improved approach is achieved when using (13) or (14):

$$\exists\left\{\left(\Xi_{\lambda\, i,(j-1)} \equiv LOG1\right) \in \left(B_{C1} \cup B_{C2}\right)\right\} \equiv \lambda_{FBG\,i,(j-1)} \Rightarrow$$

$$\Rightarrow \begin{cases} \forall\left\{\lambda_{FBG\,i,(j-2)} > \lambda_{FBG\,i,(j-1)}\right\} \therefore \left\{\Xi_{\lambda_{FBG}\,(i-k),\,j} \ldots \Xi_{\lambda_{FBG}\,i,\,j}\right\} \equiv LOG1 \\ \forall\left\{\lambda_{FBG\,i,(j-2)} < \lambda_{FBG\,i,(j-1)}\right\} \therefore \left\{\Xi_{\lambda_{FBG}\,i,\,j} \ldots \Xi_{\lambda_{FBG}\,(i+k),\,j}\right\} \equiv LOG1, \end{cases} \tag{13}$$

$$\forall\left\{\Xi_{TChs\ (o\in(1\ldots32)),\,j}\right\} \equiv LOG1 \Rightarrow$$

$$\Rightarrow \begin{cases} \forall\left\{\lambda_{FBG\,i,(j-2)} > \lambda_{FBG\,i,(j-1)}\right\} \therefore \left\{\Xi_{TChs\,(o+(1\ldots r)),\,j}\right\} \equiv LOG1 \\ \forall\left\{\lambda_{FBG\,i,(j-2)} < \lambda_{FBG\,i,(j-1)}\right\} \therefore \left\{\Xi_{TChs\,(o-(1\ldots r)),\,j}\right\} \equiv LOG1. \end{cases} \tag{14}$$

5. Matrix $\Psi_{TChs\,j}$ in (15) estimates the TChs availability for a j^{th} sensing period:

$$\begin{cases} \forall\left\{\Xi_{TChs\,1\ldots32,\,j}\right\} \equiv LOG1 \ \therefore \ \forall\left\{\Psi_{TChs\,1\ldots32,\,j}\right\} \equiv LOG0 \\ \forall\left\{\Xi_{TChs\,1\ldots32,\,j}\right\} \equiv LOG0 \ \therefore \ \forall\left\{\Psi_{TChs\,1\ldots32,\,j}\right\} \equiv LOG1. \end{cases} \tag{15}$$

6. Besides of the acceptable occupancy $\Xi_{TChs\ \%\,j}$ and availability $\Psi_{TChs\ \%\,j}$ (note: $\Xi_{TChs\ \%\,j} + \Psi_{TChs\ \%\,j} = 100$ %), the quality of the available TChs should be validated by another criterion. Any post-detection residual power exceeding the $\tau_{dB\ (j-1)}$ indicates wrong settings of constants, variables, weights etc., or non-applicability of chosen steps 2. and 4. The residual noise $N_{dB\ res\ i,j}$ and threshold $\tau_{dB\ (j-1)}$ are related as follows:

$$\forall\left\{\Psi_{TChs\,1\ldots32,\,j} \equiv LOG1 \wedge \frac{N_{dB\ res\ i,j}}{\tau_{dB(j-1)}} < 1\right\} \Rightarrow \left\{\Psi_{TChs\,1\ldots32,\,j}\right\}\ is\ OK. \tag{16}$$

Note: Purposely increased $\tau_{dB\ (j-1)}$ may improve validity of chosen approach but also can increase the residual noise and worse *SNR* in TChs. On the other hand, accidentally raised noise may cause unwanted rejection of the applied approach.

IV. Simulation Results, Discussion and Validation

Our experimental models and simulation results are based on real sensing data obtained from local optical sensor network, using components like G.652.D SM OF [24], OSA and FBG sensors [25]. Their parameters are listed in Table I. Simulation results are based on the FBG sensing data set shown in Fig. 4, obtained during 45 periods i.e. 45 × 2 = 90 s.

Fig. 5 serves as a reference of occupancy example. The A, B, C, D FBGs are detected by constant threshold $\tau_{dB} = -68$ dB, based on the approaches 1.a., 2.a., 3., without estimating prohibited neighbors. Wavelengths detected above τ_{dB} are indicated by *LOG*1 in Fig. 5(a). If any occupied wavelength occurs inside of the TCh, the entire TCh is considered occupied, Fig. 5(b). Occupied 1st to 16th TChs are inside of the dashed red grouping rectangle and similarly 17th to 32nd TChs in the dashed blue rectangle. The 258 i.e. 17.92 % of total number of 32 × 45 = 1440 TChs are occupied. From those, the A-FBG (close to the 32nd TCh) does not occupy any TCh. The B-FBG occupies 92 TChs. The C-FBG occupies 67 TChs and additionally, it continuously occupies the guarding channel with 1 to 3 wavelengths. The D-FBG occupies 101 TChs by its $n_{\lambda\ D\text{-}FBG} \approx 14$ number of wavelengths.

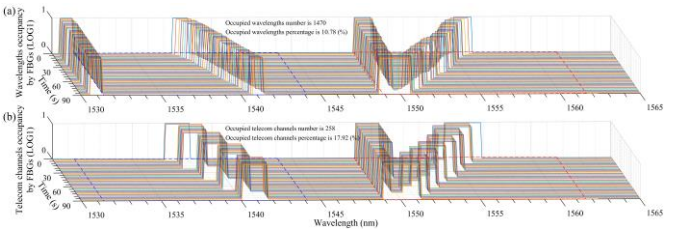

Fig. 5. Reference post-period TChs occupancy detected at constant threshold $\tau_{dB} = -68$ dB: (a) wavelengths occupancy, (b) TChs occupancy.

Fig. 6 shows the occupancy after detection by weighted variable threshold ($\tau_{dB\ (j-1)} = var$), using approaches 1.b., 2.b., 3., without estimating prohibited neighbors. In this process, the noise outliers of the previous period were localized and eliminated. Weighted noise deviation was added, thus the variable threshold $\tau_{dB\ (j-1)}$ ranges from – 69.51 to – 68.49 dB, as can be seen in Fig. 6(a). Achieving extended occupancy brings higher reliability due to non-overlapping TChs during next j^{th} period, as shown in Fig. 6(b) and 6(c).

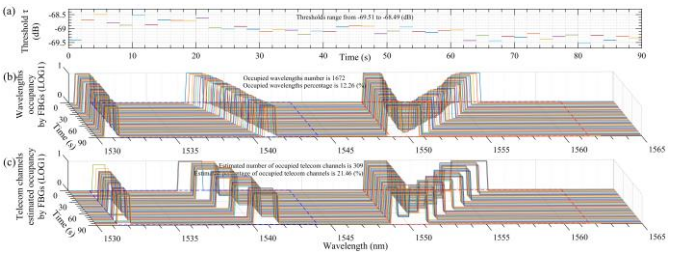

Fig. 6. Post-period TChs occupancy detected at variable threshold $\tau_{dB\ (j-1)}$ with weighted noise deviation: (a) variable threshold $\tau_{dB\ (j-1)}$ evolution, (b) wavelengths occupancy, (c) TChs occupancy.

In Fig. 7(a) ($\tau_{dB} = -68$ dB), possible unexpected FBGs shifts are up to ± 10 wavelengths bilaterally. Thus, the fixed ± 10 guard wavelengths around FBGs occupancies are estimated to be prohibited by approach 4.a. The estimated TChs occupancy is 36.04 %, Fig. 7(b), and the availability is 63.96 %, Fig. 7(c). This approach securely estimates sufficient next-period TChs availability even in the cases of possible unexpected shifts of FBGs peaks. But, its static setting of a fixed large number of guard wavelengths still represents some wasted bandwidth.

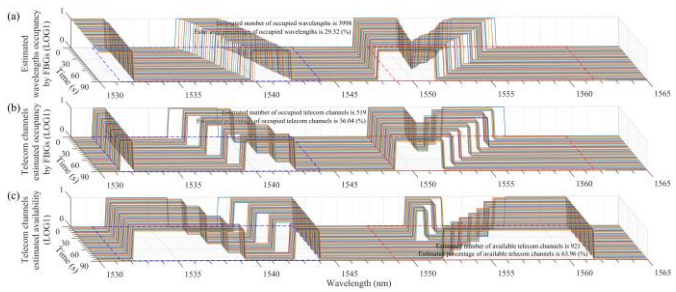

Fig. 7. Estimated TChs occupancy and availability, based on constant threshold $\tau_{dB} = -68$ dB detection and single-period estimation with respect of prohibited 10 + 10 neighboring wavelengths: (a) estimated wavelengths occupancy, (b) estimated TChs occupancy, (c) estimated TChs availability.

Similarly, in Fig. 8 ($\tau_{dB} = -68$ dB), expected FBGs shifts are up to ± 1 TChs bilaterally. Based on this coarse-grained step approach 4.b., besides of referenced 258 occupied TChs in Fig. 5(b), the 1 + 1 fixed guard TChs (i.e. additional two 100 GHz adjacent TChs) are estimated to be prohibited. The results are similar to Fig. 7, because $n_{\lambda\ TCh} \approx 10$.

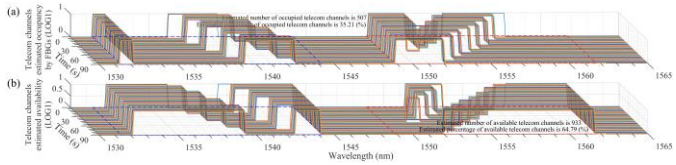

Fig. 8. Estimated TChs occupancy and availability, based on constant threshold $\tau_{dB} = -68$ dB detection and single-period estimation with respect of prohibited 1 + 1 adjacent TChs: (a) estimated TChs occupancy, (b) estimated TChs availability.

The Fig. 9 example ($\tau_{dB} = -68$ dB) respects the dynamics of FBGs. Their directions and speeds are obtained from two previous periods. Based on approach 4.c., FBGs inter-period shifts are indicated by speed values from 1 to 5 determined at FBGs power spectral peak maximum $\lambda_{Pmax\ i,j}$ shown in Fig. 9(a). The static behavior corresponds to speed value 1. The shift of 1 wavelength is indicated by speed value of 2, etc. In comparison with Fig. 8(a) and 8(b), availability of TChs in Fig. 9 (b) and 9(c) significantly increases more than 16 % thus reducing waste of bandwidth. To prove the validity of the used approach, residual noise is compared to the reference limit of – 68 dB in Fig. 9(d) according to the step 6. The background noise including the FBGs residual noise outside of the occupied, prohibited TChs and guarding zones is securely below the reference limit. Note that the higher the edge step between the noise residues and the reference limit level, the greater is the reserve in case of possible unexpected FBGs shifts. This highly reliable approach is suitable if sensing dynamics and/or lot of upstream requests are expected.

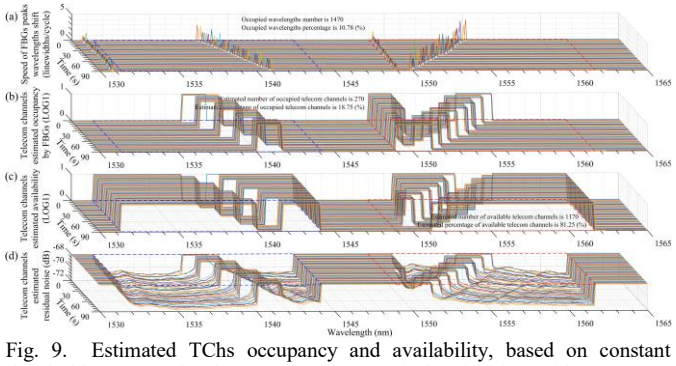

Fig. 9. Estimated TChs occupancy and availability, based on constant threshold $\tau_{dB} = -68$dB detection and two-period estimation with respect to FBGs dynamics: (a) speed of FBGs shifts, (b) estimated TChs occupancy, (c) estimated TChs availability, (d) estimated residual noise.

The Fig. 10 example implements the variable threshold and FBGs dynamics, to improve the detection of slow shift of A, B, C, D FBGs, compare Fig. 10(c) with Fig. 9(b). This results in slightly less TChs availability, see Fig. 10(d), but providing enlarged prohibited guard zones thus higher reliability. Fig. 10(e) shows that the residual noise is securely below the stricter reference limit of – 68.5 dB, bringing improved *SNR* to TChs. This approach is well suitable if sensing dynamics or lot of upstream requests are expected.

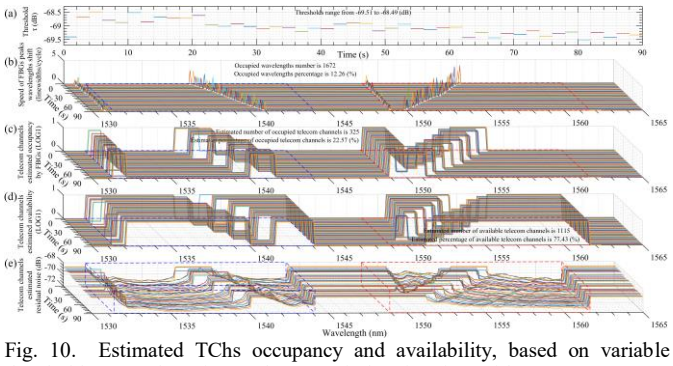

Fig. 10. Estimated TChs occupancy and availability, based on variable threshold $\tau_{dB\ (j-1)}$ detection and two-period estimation with respect to FBGs dynamics: (a) variable $\tau_{dB\ (j-1)}$ evolution, (b) speed of FBGs peaks, (c) estimated TChs occupancy, (d) estimated TChs availability, (e) estimated residual noise.

Fig. 11 is a summary of conventional and novel approaches, in order to increase the number of accessible TChs for TS. The proposed 6-step concept was applied to the multi-period 4-FBG sensing shown in Fig. 4, with the following results. The red values already account for $\Xi_{TChs\ laser\ \%} = 3.125$ % which is related to the presence of the scanning laser signal in TChs due to wavelength sweep of the laser. Fig. 11 bar (a) shows only 15.6 % of TChs availability for TS when conventional approach was applied. Fig. 11 bars (b), (c), (d), (e) are grouped in dashed purple rectangle that show 4 times higher TChs availability thanks to implemented constant thresholding described in step 2.a. and bilateral prohibition described in steps 4.a. and 4.b. Fig. 11 bar (f) shows improved TChs availability up to 75.4 % but with less certainty resulted from a possible unexpected FBGs shift (represented by white color gap) when a threshold detection from step 2. is implemented with no adjacent prohibition. Fig. 11 bars (g) and (h) show the highest TChs availability (rising nearly 5 times, approaching 80 %). This has been achieved by implementing threshold detection from step 2. with unilateral prohibiting approach from step 4.c. One can

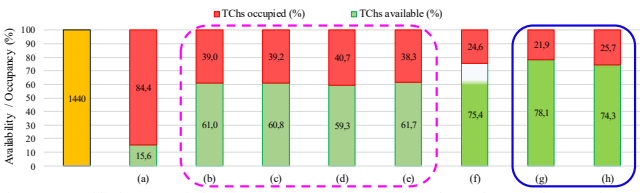

Fig. 11. Efficiency of the four FBGs case study when the total wavelengths number is 1440 using: (a) conventional approach with permanent FBG operational windows, (b) constant thresholding ($\tau_{dB} = -68$ dB) with respect of prohibited 9 + 9 neighboring wavelengths, (c) constant thresholding with respect of prohibited 10 + 10 neighboring wavelengths, (d) constant thresholding with respect of prohibited 13 + 13 neighboring wavelengths, (e) constant thresholding with respect of prohibited 1 + 1 adjacent TChs, (f) variable thresholding ($\tau_{dB\ (j-1)} = -69.51 \ldots -68.89$ dB) without prohibited neighboring wavelengths, (g) constant thresholding with respect to FBGs dynamics, (h) variable thresholding with respect to FBGs dynamics.

see, the dynamic thresholding (Fig. 11(h)) delivers slightly less available TChs (compared to constant threshold, Fig. 11(g)). On the other hand, it brings more favorable background noise distribution and thus better *SNR*.

V. Conclusion

A conventional approach uses fixed FBG operational wavelengths windows and does not allow to share them with telecommunications services (TS) thus is wasting the bandwidth. This paper introduces for the first time a novel concept of sharing bandwidth between an FBG sensing and TS. It includes mathematical simulations and experimental results. The proposed 6-step concept uses FBGs power spectral peaks statistical detection, monitoring of the FBGs dynamics and periodic estimation of telecommunication channels (TChs) occupancy and availability. Various approaches were experimentally demonstrated to improve TChs occupancy and availability in the FBG sensing.

In our 4-FBGs-based sensing case study, the conventional approach offered only 15.6 % of TChs available for TS. However, by implementing our novel concept, the FBG sensing and telecommunications services will share common bandwidth. To implement this, a rigorous thresholding and bilateral TChs prohibition will guarantee the TChs availability to rise 4 times i.e. up to 62 %. When implementing unilateral prohibiting approach, the TChs availability rises 5 times, approaching 80 %. The latter brings higher certainty of TChs not interfering with FBGs peaks. Future work could include the dynamic bandwidth allocation management.

References

[1] G. Keiser, „Fiber Optic Communication Networks", in Fiber Optic Communication, corrected ed., Singapore, Springer, 2021, pp. 507-575. [Online] DOI 10.1007/978-981-33-4665-9.

[2] X. Bai, A. Shami and C. M. Assi, "On the fairness of dynamic bandwidth allocation schemes in Ethernet passive optical networks", *Comp. Comm.*, vol. 29, no. 11, pp. 2123–2135, July 2006, DOI 10.1016/j.comcom.2006.01.005.

[3] X. Bai, A. Shami, and C. M. Assi, "Statistical bandwidth multiplexing in Ethernet passive optical networks", *Proc. IEEE GLOBECOM 2005*, pp. 1920-1924 [Online]. DOI 10.1109/GLOCOM.2005.1578001.

[4] B. Skubic, J. Chen, J. Ahmed, L. Wosinska, and B. Mukherjee, "A comparison of dynamic bandwidth allocation for EPON, GPON, and Next-Generation TDM PON", *IEEE Comm. Magazine*, vol. 47, no. 3, pp. 540-548, March 2009, DOI 10.1109/MCOM.2009.4804388.

[5] T. Horvath, P. Munster, V., Oujezdsky, and N.-H. Bao, "Passive optical networks progress: a tutorial", *Electronics*, vol. 9, no. 7, p. 31, July 2020, DOI 10.3390/electronics9071081.

[6] A. Shao, Q. Dou, Y. Xiao, P. Chu, K. Zhi, Y. Peng, and K. Long, "Bandwidth allocation design to guarantee QoS of differentiated services for a novel OFDMA-PON", *Proc. IEEE APCC 2012*, pp. 775-780 [Online]. DOI 10.1109/APCC.2012.6388213

[7] I. N. Cano, X. Escayola, Á. Peralta, V. Polo, M. C. Santos, and J. Prat, "A study of flexible bandwidth allocation in statistical OFDM-based PON", *Proc. IEEE ICTON 2013*, p. 4 [Online]. DOI 10.1109/ICTON.2013.6602853

[8] I. N. Cano, X. Escayola, P. C. Schindler, M. C. Santos, V. Polo, J. Leuthold, I. Tomkos, and J. Prat, "Experimental demonstration of a statistical OFDM-PON with multiband ONUs and elastic bandwidth allocation", *J. Opt. Comm. Netw.*, vol. 7, no. 1, pp. A73-A79, Jan. 2015, DOI 10.1364/JOCN.7.000A73.

[9] C. Ni, Ch. Gan, W. Li, and H. Chen, "Bandwidth allocation based on priority and excess-bandwidth-utilized algorithm in WDM/TDM PON", *AEU – Int. J. Electron. Comm.*, vol. 69, no. 11, pp. 1659-1666, Nov. 2015, DOI 10.1016/j.aeue.2015.07.020.

[10] J. Segarra, V. Sales, J. Prat, "Grade of service in UDWDM-PON with statistical wavelength subscribing", *Proc. IEEE EuCNC 2018: WOS*, pp. 383-387 [Online]. DOI 10.1109/EuCNC.2018.8443244.

[11] W. Lim, P., Kourtessis, J. M. Senior, Y. Na, Y, Allawi, S.-B. Jeon, and H. Chung, "Dynamic bandwidth allocation for OFDMA-PONs using hidden Markov model", *Opt. Eng.*, vol. 56, no. 3, pp. 21016-21019, Feb. 2017, DOI 10.1109/ACCESS.2017.2657549.

[12] K. A. Memon, K, H. Mohammadani, A. A. Laghari, R. Yadav, B. Das, W. U. K. Tareen, N. A. Memon, and X. Xin, "Dynamic bandwidth allocation algorithm with demand forecasting mechanism for bandwidth allocations in 10-gigabit-capable passive optical network", *Optik*, vol. 183, pp. 1032-1042, Apr. 2019, 10.1016/j.ijleo.2019.03.003.

[13] K. A. Memon, K, H. Mohammadani, N. Ain, A. Shaikh, S. Ullah, Q. Zhang, B. Das, R. Ullah, F. Tian, and X. Xin, "Demand forecasting DBA algorithm for reducing packet delay with efficient bandwidth allocation in XG-PON", *Electronics MDPI*, vol. 8, no. 147, p. 13, Jan. 2019, DOI 10.3390/electronics8020147.

[14] R. A. Butt, M. Faheem, and M. W. Ashraf, „Efficient upstream bandwidth utilization with minimum bandwidth waste for time and wavelength division passive optical network", *Opt. Quantum Electron.*, vol. 52, no. 14, p. 26, Dec. 2019, 10.1007/s11082-019-2127-y.

[15] K. Wang, S. Qi, Z. Chen, and H. Gu, "SMONoC: Optical network-on-chip using a statistical multiplexing strategy", *Opt. Switch. Netw.*, vol. 34, p. 9, Nov. 2019, DOI 10.1016/j.osn.2019.03.004.

[16] B. Cao, X. Zheng, K. Yuan, D. Qin, and Y. Hong, "Dynamic bandwidth allocation based on adaptive predictive for low latency communications in changing passive optical networks environment", *Opt. Fiber Technol.*, vol. 64, p. 9, July 2021, DOI 10.1016/j.yofte.2021.102556.

[17] A. Rafiq, M. F. Hayat, and M. U. Younus, "Dynamic bandwidth allocation algorithm for avoiding frame rearrangement in NG-EPON", *Opt. Switch. Netw.*, vol. 43, p. 8, Feb. 2022, DOI 10.1016/j.osn.2021.100645.

[18] S. Garg, and A. Dixit, "Bin-packing based offline dynamic bandwidth and wavelength allocation algorithms for power efficiency in Super-PON", *OSA Continuum*, vol. 4, no. 8, pp. 2091-2107, 2021, DOI 10.1364/OSAC.430997.

[19] IEEE Standard for Ethernet, IEEE Std 802.3-2018 (Revision of IEEE Std 802.3-2015), 2018.

[20] IEEE Standard for Ethernet amendment 9: Physical layer specifications and management parameters for 25 Gb/s and 50 Gb/s passive optical networks", IEEE Std 802.3ca-2020, 2020.

[21] IEEE Increased-reach Ethernet optical subscriber access (Super-PON), IEEE P802.3cs, 2022.

[22] C. DeSanti, L. Du, J. Guarin, J. Bone, and C. F. Lam, "Super-PON: an evolution for access networks", *J. Opt. Commun. Netw.*, vol. 12, no. 10, pp. D66-D77, Oct. 2020, DOI 10.1364/JOCN.391846.

[23] L. B. Du, X. Zhao, S. Yin, T. Zhang, A. E. T. Barratt, J. Jiang, D. Wang, J. Geng, C. DeSanti, and C. F. Lam. "Long-reach wavelength-routed TWDM PON: technology and deployment", *J. Light. Technol.*, vol. 37, no. 3, pp. 688-697, Feb. 2019, DOI10.1109/JLT.2018.2850343.

[24] Characteristics of a single-mode optical fibre and cable, Recommendation ITU-T G.652, 2019.

[25] Sensing systems. Sylex s.r.o., Bratislava, Slovakia [Online]. Available: https://www.sylex.sk/products/sensing-systems/

[26] K. Kasai, M. Nakazawa, Y. Tomomatsu, and T. Endo, "1.5μm, mode-hop-free full C-band wavelength tunable laser diode with a linewidth of 8 kHz and a RIN of −130 dB/Hz and its extension to the L-band," *Opt. Express*, vol. 25, no. 18, pp. 22113-22124, Sept. 2017, DOI 10.1364/OE.25.022113.

[27] F. Yang, W. Zhang, S. Zhao, Q. Liu, J. Tao, and Z. He, "Miniature interrogator for multiplexed FBG strain sensors based on a thermally tunable microring resonator array," *Opt. Express*, vol. 27, no. 4, pp. 6037-6046, Mar. 2019, DOI 10.1364/OE.27.006037.

[28] C. K. Ha, K. S. Lee, D. Kwon, and M. S. Kang, "Widely tunable ultra-narrow-linewidth dissipative soliton generation at the telecom band," *Photon. Res.*, vol. 8, no. 7, pp. 1100-1109, July 2020, DOI 10.1364/PRJ.389080.

[29] X. Liu, X. Yan, Y. Liu, H. Li, Y. Chen, and X. Chen, "Tunable single-mode laser on thin film lithium niobate," *Opt. Lett.*, vol. 46, no. 41, pp. 5505-5508, Aug. 2021, DOI 10.1364/OL.441167.

[30] Y. Su, T. Zhao, X. Wang, S. Liu, "Design of feedback wavelength demodulation and compensation system for FBG-tuned CW fiber laser", *Sens. Actuators A: Phys.*, vol. 330, p. 7, Oct. 2021, DOI 10.1016/j.sna.2021.112881.

[31] A. D. Kersey, M. A. Davis, H. J. Patrick, M. Leblanc, K. Koo, C. G. Askins, M. Putnam, and E. Friebele, "Fiber grating sensors", *J. Light. Technol.*, vol. 15, no. 8, pp. 1442–1463, Aug. 1997, DOI 10.1109/50.618377.

[32] T. Erdogan, "Fiber grating spectra", *J. Light. Technol.*, vol. 15, no. 8, pp. 1277–1294, Aug. 1997, DOI 10.1109/50.618322.

[33] K. O. Hill, and G. Meltz, "Fiber Bragg grating technology fundamental and overview", *J. Light. Technol.*, vol. 15, no. 8, pp. 1263–1276, Aug. 1997, DOI 10.1109/50.618320.

[34] M. F. Bado, J. R. Casas, "A review of recent distributed optical fiber sensors applications for civil engineering structural health monitoring", *Sensors MDPI*, vol. 21, no. 5, p. 83, 2021, DOI 10.3390/s21051818.

[35] Y. Guo, Ch. Yu, Y. Ni, and H. Wu, "Accurate demodulation algorithm for multi-peak FBG sensor based on invariant moments retrieval", *Opt. Fiber Technol.*, vol. 54, no. 9, Jan. 2020, 10.1016/j.yofte.2019.102129.

[36] C. Fernández-Valdivielso, I. R. Matías, and F. J. Arregui, "Simultaneous measurement of strain and temperature using a fiber Bragg grating and a thermochromic material", *Proc. at IEEE OFS 2002*, vol. 101, no. 1-2, pp. 203-206, DOI 10.1109/OFS.2002.1000537.

[37] J. He, Z. Zhou, and K. Ou, "Simultaneous measurement of strain and temperature using a hybrid local and distributed optical fiber sensing system", *Measurement*, vol. 47, pp. 698-706, Jan. 2014, DOI 10.1016/j.measurement.2013.10.006

[38] A. Masoudi, and T. P. Newson, "High spatial resolution distributed optical fiber dynamic strain sensor with enhanced frequency and strain resolution" *Opt. Lett.*, vol. 42, no. 2, pp. 290-293, Jan. 2017, DOI 10.1364/OL.42.000290.

[39] C. E. Campanella, A. Cuccovillo, C. Campanella, C., A. Yurt, and V. M. N. Passaro, "Fibre Bragg grating based strain sensors: review of technology and applications", *Sensors MDPI*, vol. 18, no. 9, p. 27, Sept. 2018, DOI 10.3390/s18093115.

[40] Ch. Li, J. Tang, Ch. Cheng, and M. Yang, "FBG arrays for quasi-distributed sensing: a review", *Photonic sens.*, vol. 11, no. 1, pp. 91-108, Jan. 2021, DOI 10.1007/s13320-021-0615-8.

[41] P. Lu, N. Lalam, M. B. Liu, B. T. Chorpening, M. P., Buric, and P. R. Ohodnicki, "Distributed optical fiber sensing: review and perspective", *Appl. Phys. Rev.*, vol. 6, no. 4, p. 34, Oct. 2019, 10.1063/1.5113955.